Unitarity Corrections and a Four-Pole Fit to Peripheral p-p Scattering below 350 MeV*

R. A. ARNDT, R. A. BRYAN, AND M. H. MACGREGOR
Lawrence Radiation Laboratory, University of California, Livermore, California
(Received 21 April 1966)

Proton-proton partial-wave amplitudes for $l\geq 1$ and for lab kinetic energies below 350 MeV are fitted with a collection of single-particle exchanges taken in Born (fixed-pole) approximation. Since the Born terms are real, and consequently nonunitary, a correction term is added which makes the full amplitude unitary, and which at the same time satisfies the appropriate dispersion relation and threshold condition. The nature of this correction term and of its association with a strip approximation to the Mandelstam representation are discussed. The particle parameters were fitted to a reduced matrix representation of the p-p data, as described by Arndt and MacGregor in another publication. The S-wave dependence was removed in a manner also discussed by these authors. The gross structure of the partial-wave amplitudes is found to be approximately given by a sum of four meson-exchange poles, those corresponding to a π meson ($J^P=0^-$, $I=1$, $g_\pi^2=14$, $M_\pi=135$ MeV), a σ meson ($J^P=0^+$, $I=0$, $g_\sigma^2=2.9$, $M_\sigma=450$ MeV), an ω meson ($J^P=1^-$, $I=0$, $g_\omega^2=4$, $(f/g)_\omega=0$, $M_\omega=783$ MeV), and a ρ meson ($J^P=1^-$, $I=1$, $g_\rho^2=1.2$, $(f/g)_\rho=4$, $M_\rho=763$ MeV). The searched parameters were g_π^2, g_σ^2, g_ω^2, g_ρ^2, and M_σ; the remaining parameters were fixed at their "physical" values. It is further found that the relatively small unitarizing corrections play an essential role in determining the goodness of fit, but they do not appreciably alter the pole parameters determined from the search. Studies were also undertaken to determine the manner in which this (obviously low-energy) model becomes quantitatively worse as low-angular-momentum and high-energy contributions are added to the calculation.

I. INTRODUCTION

THE model with which we attempt to describe the two-proton problem is for a region of incident energies in which the low-energy partial-wave amplitudes for $l\geq 1$ are dominated by single-particle exchanges—bound states and resonances in the cross channels. We represent each of the "particles" by a fixed pole in momentum transfer (energy in the $p\bar{p}$ channel). It is well known, however, that the partial-wave projections for fixed, cross-channel poles are real in the physical ($T>0$, T=lab kinetic energy) region, and thus nonunitary. Thus one problem is to restore unitarity without destroying the threshold behavior.

If we consider the partial wave amplitude $h_l(T)$ to be a function of a complex laboratory-frame kinetic-energy variable T, we find it has the following singularity structure:

(1) A right-hand cut (the physical or unitarity cut) which runs from $T=0$ to $T=\infty$. This cut is a consequence of unitarity in the p-p channel;

(2) A left-hand cut (often referred to as the potential or driving-term cut) which extends from $T=-\mu^2/2M$ to $T=-\infty$, where μ=pion mass and M=nucleon mass.

Expressing, through the Cauchy relations, the amplitude in terms of its singularities, we obtain

$$h_l(T)=\frac{1}{2\pi i}\int_0^\infty \frac{D_R(T')dT'}{T'-T}+\frac{1}{2\pi i}\int_{-\infty}^{-T_L'} \frac{D_L(T')dT'}{T'-T}, \quad (1.1)$$

where

$$T_L'=\mu^2/2M,$$

and where $D_R(T)$ and $D_L(T)$ are the discontinuities in $h_l(T)$ along the right and left cuts, respectively. Further, since the amplitude is real for $(-T_L'<T<0)$, we can use Hermitian analyticity $[h_l^*(T)=h_l(T^*)]$ to obtain

$$D_l(T)=2i\,\mathrm{Im}h_l(T),$$

which allows us to rewrite (1.1) as

$$h_l(T)=\frac{1}{\pi}\int_0^\infty \frac{\mathrm{Im}h_l(T')dT'}{T'-T}+\frac{1}{\pi}\int_{-\infty}^{-T_L'} \frac{\mathrm{Im}h_l(T')}{T'-T}dT'. \quad (1.2)$$

Partial-wave projections of contributions from fixed cross-channel poles, referred to henceforth as $B_l(T)$, also satisfy an equation having the structure of (1.2), but they have no right-hand cut since $\mathrm{Im}B_l(T)=0$, $T>0$. The calculations are carried out by making use of a decomposition of the amplitude into a Born term, $B(T)$, and a remainder term, $U(T)$:

$$h(T)=B(T)+U(T), \quad (1.3)$$

where the subscript l is now suppressed.

For reasons that will be discussed in Sec. II, we introduce a cutoff T_1 into the right-hand integral for $h(T)$, and associate the right-hand cut in $h(T)$ for $T>T_1$ with $B(T)$; that is,

$$B(T)=\frac{1}{\pi}\int_{-\infty}^{-T_L'} \frac{\mathrm{Im}B(T')dT'}{T'-T}+\frac{1}{\pi}\int_{T_1}^\infty \frac{\mathrm{Im}h(T')}{T'-T}dT'. \quad (1.4)$$

Justification for treating $B(T)$ in the low-energy ($0<T<350$ MeV) region as a sum of fixed poles will be given in Sec. II.

Combining Eqs. (1.2)–(1.4), we obtain a dispersion relation for $U(T)$:

$$U(T)=\frac{1}{\pi}\int_0^{T_1} \frac{\mathrm{Im}h(T')}{T'-T}dT'+\frac{1}{\pi}\int_{-\infty}^{-T_L} \frac{\mathrm{Im}U(T')}{T'-T}dT', \quad (1.5)$$

* Work performed under the auspices of the U. S. Atomic Energy Commission.

where $T_L=2\mu^2/M$, corresponding to the 2π threshold, since the single-pion-exchange cut is included in $B(T)$. An important requirement for $h(T)$ is the threshold behavior

$$h_l(T)\propto T_l \quad \text{as} \quad T\to 0. \tag{1.6}$$

Since this behavior is satisfied by our fixed-pole approximation to $B(T)$, we will require it of $U(T)$. That is, $U(T)$ must satisfy

$$U(T)=\frac{T^l}{\pi}\int_0^{T_1}\frac{\mathrm{Im}h(T')dT'}{T'^l(T'-T)} +\frac{T^l}{\pi}\int_{-\infty}^{-T_L}\frac{\mathrm{Im}U(T')}{T'^l(T'-T)}dT', \tag{1.7}$$

with subsidiary conditions

$$\int_0^{T_1}\frac{\mathrm{Im}h(T')}{T'^n}dT'=-\int_{-\infty}^{-T_L}\frac{\mathrm{Im}U(T')}{T'^n}dT', \qquad n=1,\cdots l.$$

Our procedure for unitarizing the Born amplitudes is to try various constructs for $\mathrm{Im}U(T)$ $(T<-T_L)$ that satisfy the subsidiary conditions of (I7). From $\mathrm{Im}U(T)$ we obtain $U(T)$ through Eq. (I5), where $\mathrm{Im}h(T')$ is taken from experiment.[1] Finally, through Eq. (I3), we fit $B(T)=h(T)-U(T)$ with a suitable choice of poles. It should be emphasized that in this analysis both h and U are experimental quantities. This procedure is self-consistent if we obtain a reasonable solution for $B(T)$, since we can always go back and construct $\mathrm{Im}h$ (through unitarity) from h and thereby reconstruct a self-consistent $U(T)$.

Our approach differs from Kantor[2] and from Scotti and Wong[3] principally in the inclusion in $B(T)$ of all the high-energy behavior for $h(T)$. The association of $U(T)$ with the direct-channel strips in a strip approximation to the Mandelstam representation to the amplitude is discussed in Sec. II.

The approach differs further from Kantor, as discussed by MacGregor,[4] in the philosophy of treatment for the left cut of $U(T)$. Kantor builds the appropriate threshold behavior into $U(T)$, but ignores that part of Eq. (I7) which comes from integrating over the left cut. We, on the other hand, treat it in a semiphenomenological way by constructing various left-hand cuts for $U(T)$ which satisfy the subsidiary conditions to Eq. (I7), and which may include some undetermined (free) parameters. $U(T)$ is then constructed and poles

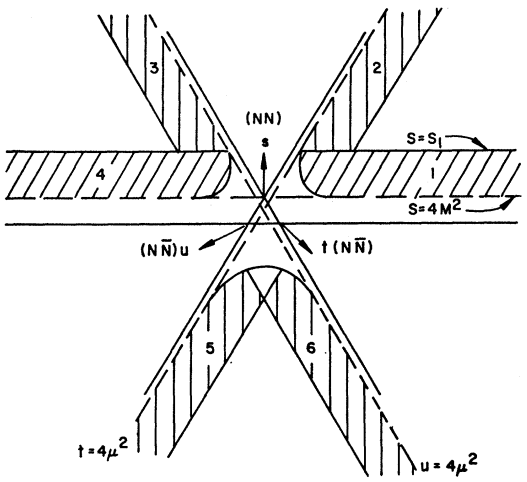

FIG. 1. Strip approximation to Mandelstam representation for N-N scattering amplitude.

are fit, as was previously described. The Kantor-type correction, a subtracted integral over the right-hand cut, but including the T_1 cutoff, is also tried as a limiting case of an approximation to $U(T)$ described in Sec. IIB (approximation A). The result is tabulated and compared to other approximations.

Scotti and Wong represent the left-hand cut in $U(T)$ by an $(l-1)^{\text{st}}$ order pole at some reasonably large negative energy, with the residues arranged so as to satisfy the subsidiary conditions of (I7). They do not include a cutoff in their right-hand integral.

Finally, we include, for comparison, simple pole fits to the (nonunitarized) amplitudes $\mathrm{Re}h^{\text{exp}}(T)$, $(U(T)=0)$. This is the same model as that defined by Bryan and Arndt.[5]

II. THE UNITARITY TERM

A. General Discussion

The fundamental assumption in our approximate treatment of unitarity will be that the nucleon-nucleon amplitudes, denoted collectively as $A(s,t,u)$, satisfy a strip approximation to the Mandelstam representation, where s, t, and u are the energy-squared variables in the NN channel and crossed $N\bar{N}$ channels, respectively. That is, we consider only those regions of the double spectral function indicated in Fig. 1. (Figure 1 shows a Mandelstam plot where the one-pion-exchange singularity is not included.) We make a separation of the amplitude into the part obtained by integrating over the cross-channel strips (labeled 2, 3, 5, 6 in Fig. 1), which we call $V(s,t,u)$, the "potential" term, and the part obtained by integrating over the direct-channel strips (labeled 1, 4 in Fig. 1), which we denote as $U(s,t,u)$, the unitarity term.

It is significant that the resonances (poles) in the $N\bar{N}(t)$ channel are "contained" in the double spectral

[1] R. A. Arndt and M. H. MacGregor, Phys. Rev. **141**, 875 (1966); referred to as AM. Obtaining an expression for the χ^2 correlation matrix which does not depend explicitly on data normalization parameters was also accomplished by G. Breit, A. N. Christakis, M. H. Hull, Jr., H. M. Ruppel, and R. E. Seamon, in *Proceedings of the 12th Annual International Conference on High-Energy Physics, Dubna, 1964* (Atomizdat, Moscow, 1965), Vol. I, p. 17.

[2] P. B. Kantor, Phys. Rev. Letters **12**, 52 (1964).

[3] A. Scotti and D. Y. Wong, Phys. Rev. Letters **10**, 142 (1963); Phys. Rev. **138**, B145 (1965).

[4] M. H. MacGregor, Phys. Rev. Letters **12**, 403 (1964).

[5] R. A. Bryan and R. A. Arndt, Phys. Rev. **150**, 1299 (1966).

functions at very large s or u. To illustrate this we can calculate the $N\bar{N}$ channel discontinuity, which is

$$D_t=\frac{1}{\pi}\int_{4M^2}^{\infty}\frac{ds'}{s'-s}\rho_{st}(s',t)+\frac{1}{\pi}\int_{4\mu^2}^{\infty}\frac{du'}{u'-u}\rho_{tu}(t,u'). \quad (2.1)$$

Since the integrands are nonsingular, a resonance behavior for D_t can be achieved only by divergence of the integrals at ∞, and production of these poles should be insensitive to the precise lower limits chosen in Eq. (2.1). This argument for the occurrence of the poles in the distant parts of the double spectral functions is equally valid for stable (e.g., the π meson) and for unstable (e.g., the ρ meson) poles. We see, then, that the low-mass resonances in the $N\bar{N}$ channel are contained in the cross-channel strips, and therefore are part of the "potential," $V(s,t,u)$. It will be our approximation to keep only the resonant parts of V.

Since we have excluded the nearby s discontinuities from our definition of the "potential," we have left the low-s, -t, -u regions of the Mandelstam diagram for the potential V (Fig. 1 with strips 1 and 4 excluded) free of singularities. We expect that a partial-wave expansion of the $N\bar{N}$ channel amplitude, that is, a polynomial expansion in s ($s\sim\cos\theta_t$, with θ_t the $N\bar{N}$-channel scattering angle), can be analytically continued to the low-energy region of the NN channel. A low-energy (NN-channel) fixed-pole approximation is equivalent to replacing the $N\bar{N}$-channel partial-wave sum by only the resonating terms, taken in a zero-width approximation. Thus, our approximation to V (the "potential") is to represent it as a collection of Born terms $B(T)$.

The question now confronting us is what to do with the direct-channel strip contributions, $U(s,t,u)$. We estimate these contributions by making the following approximations. The lth partial-wave projection of U is

$$U_l(T)=\frac{1}{2}\int_{-1}^{+1}U(T,z_s)P_l(z_s)dz_s, \quad (2.2)$$

where

$$T=2q_s^2/M, \quad z_s=\cos\theta_s.$$

θ_s and q_s are, respectively, the c.m. angle of scattering and the c.m. momentum of either nucleon in the NN channel. We will use two different approximations to $U_l(T)$. These we label A and B. They are discussed in Secs. IIB and IIC. Our approximations will avoid explicit evaluation of the double spectral functions, but will share all the characteristics described in the introduction, which may be summarized as follows:

$$\mathrm{Im}U_l(T)=\mathrm{Im}h_l(T), \quad (0<T<T_1), \quad (2.3a)$$

$$U_l(T)\propto T^l \quad \text{as} \quad T\to 0, \quad (2.3b)$$

$$\int_{-\infty}^{-T_L}\frac{\mathrm{Im}U_l(T')dT'}{T'^n}=-\int_0^{T_1}\frac{\mathrm{Im}h_l(T')dT'}{T'^n}, \quad (n=1,\cdots l). \quad (2.3c)$$

Although the approximations to be described in the following sections are very crude and differ drastically from one another at negative T, they all lead to similar results for $U_l(T)$ in the region $0<T<300$ MeV. The conditions (2.3a)–(2.3c) appear to be of overriding importance in this region.

B. Approximation A

As described in Sec. II, $U(T)$ may be expressed, through its Mandelstam representation, as

$$U(T,z_s)=\frac{1}{\pi^2}\int_{t_0}^{\infty}\frac{dt'}{t'-t}\int_0^{T_1}\frac{dT'}{T'-T}\rho(t',T), \quad (2.4)$$

where

$$t=-2q_s^2(1-\cos\theta_s)=-2q_s^2(1-z_s),$$
$$t_0=4\mu^2.$$

From Eq. (2.4) we can obtain the partial-wave projection $U_l(T)$:

$$U_l(T)=\frac{1}{2}\int_{-1}^{+1}U(T,z_s)P_l(z_s)dz_s$$
$$=\frac{1}{\pi^2MT}\int_{t_0}^{\infty}Q_l\left(1+\frac{t'}{MT}\right)dt'\times\int_0^{T_1}\frac{\rho(t',T')dT'}{T'-T}. \quad (2.5)$$

Chew[6] has suggested replacing the t' integration in Eq. (2.5) with a mean-value-type approximation. This is the approximation we call A.

$$U_l^A(T,\bar{t})=\frac{C}{\pi^2MT}Q_l\left(1+\frac{\bar{t}}{MT}\right)\int_0^{T_1}\frac{\rho(\bar{t},T')dT'}{T'-T}. \quad (2.6)$$

We require U^A to have the correct right-hand cut [Eq. (2.3a)], which enables us to solve for $\rho(\bar{t},T)$:

$$\rho(\bar{t},T)=\pi\frac{\mathrm{Im}h_l(T)MT}{CQ_l(1+\bar{t}/MT)}. \quad (2.7)$$

This expression for ρ may now be used in Eq. (2.6) to calculate U^A:

$$U_l^A(T,\bar{t})=\frac{1}{\pi}\int_0^{T_1}\frac{\mathrm{Im}h_l(T')}{T'-T}\left[\frac{T'Q_l(1+\bar{t}/MT)}{TQ_l(1+\bar{t}/MT')}\right]dT'. \quad (2.8)$$

It should be pointed out that our replacement of the t' integration in Eq. (2.5) is by no means an exact application of the mean-value theorem, but it has resulted in an approximation U_l^A which satisfies all the desired characteristics given in Eq. (2.3). The parameter $\bar{t}$ will be varied in our study and is considered as a phenomenological parameter. The A approximation,

[6] G. F. Chew (private communication).

as treated here, introduces only a single parameter $\bar{t}$ into our description of $U(T)$; however, this approximation lends itself to the introduction of any number of free (phenomenological) parameters in a way which preserves the requirements of Eq. (2.3). We can define a *total* approximation A as

$$U_l^A(T,\sigma)\equiv\sum_{k=1}^{N}\beta_k U_l^A(T,\bar{t}_k), \tag{2.9}$$

with

$$\sum_{k=1}^{N}\beta_k=1.$$

$U_l^A(T,\sigma)$ has the correct right-hand cut and threshold behavior and has, in addition, $N-1$ free parameters which may be adjusted to fit experiment.

The left-hand discontinuity associated with a particular choice of $\bar{t}$ is not needed to evaluate $U_l^A(T,\bar{t})$, but is given by

$$\mathrm{Im}U_l^A(T,\bar{t})=\tfrac{1}{2}P_l\left(1+\frac{\bar{t}}{MT}\right)\int_0^{T_1}\frac{\mathrm{Im}h_l(T')}{T'-T}\left[\frac{T'}{T}\right]\times\frac{dT'}{Q_l(1+\bar{t}/MT')}(-\infty<T<-\bar{t}/2M). \tag{2.10}$$

C. Approximation B

This approximation is similar to that suggested by MacGregor,[4] which was to construct a left-hand discontinuity $[\mathrm{Im}U_l(T)]$ which has the appropriate moments to produce the required threshold behavior:

$$\int_{-\infty}^{-T_L}\frac{\mathrm{Im}U_l^B(T')}{T'^n}dT'=-\int_0^{T_1}\frac{\mathrm{Im}h_l(T')}{T'^n}dT',\qquad n=1,\cdots l, \tag{2.11}$$

and which will be otherwise physically plausible. We will further require the left-hand cut to satisfy the appropriate threshold dependence at $T=-T_L$, as derived in Appendix I:

$$\mathrm{Im}U_l(T)\sim(T+T_L)^{3/2}\quad\text{as}\quad T\to-T_L. \tag{2.12}$$

A suitable construction for the left-hand discontinuity is

$$\mathrm{Im}U_l^B(T,j_k)=(x+1)^{3/2}(x-1)\sum_{j=j_k}^{j_k+l-1}\alpha_k x^j, \tag{2.13}$$

where

$$x=1+2T_L/T.$$

This expression maps the left-hand cut from the interval $(-\infty<T<-T_L)$ into the interval $(+1>x>-1)$. The factor $(x+1)^{3/2}$ produces the correct threshold behavior [Eq. (2.12)], and the $(x-1)$ factor forces vanishing of the discontinuity at $T=-\infty$, a requirement necessary to satisfy the first $(n=1)$ condition of

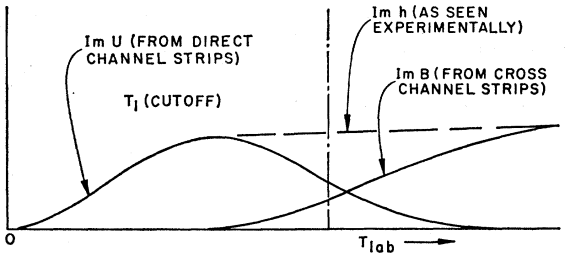

FIG. 2. Diagram relating to choice of strip width T_1 (see Sec. IID).

Eq. (2.3). The parameter j_k, which is analogous to the parameter $\bar{t}$ in approximation A, has been introduced as a means of studying the effect on $U(T)$ of varying the "structure" of the left-hand discontinuity. Introduction of the parameter j_k also allows us, as in the case of approximation A, to define a *total* correction $U_l^B(T,\sigma)$:

$$U_l^B(T,\sigma)\sum_{k=1}^{N}\beta_k U_l^B(T,j_k), \tag{2.14}$$

with

$$\sum_{k=1}^{N}\beta_k=1.$$

The coefficients α_j are determined from Eq. (2.3), and $U_l^B(T,j_k)$ is obtained from its dispersion relation:

$$U_l^B(T,j_k)=\frac{1}{\pi}\int_{-\infty}^{-T_L}\frac{\mathrm{Im}U_l^B(T',j_k)}{T'-T}dT'+\frac{1}{\pi}\int_0^{T_1}\frac{\mathrm{Im}h_l(T')dT'}{T'-T}. \tag{2.15}$$

D. Discussion of Strip Width T_1

We have introduced a cutoff T_1 into our approximation. It is associated in a natural way with the width of the direct-channel strips in our approximate Mandelstam representation. An alternative way of viewing the cutoff is to say that, in a more sophisticated approach, V (the cross-channel strip contribution) would be given by a sum of Regge poles B^R. Asymptotically, for large T, we expect these poles to determine the amplitude. That is,

$$h(T)\to B^R(T)\quad\text{as}\quad T\to\infty, \tag{2.16}$$

which, by our definition for $U(T)$, means that

$$U(T)\to 0\quad\text{as}\quad T\to\infty.$$

Thus both the strip approximation and the Regge assumption lead to the same asymptotic relationship.

The question then arises as to the exact meaning of the cutoff T_1. It is clear that, in a strip approximation, there can be no clear separation between the contributions coming from strips 1 and 2 in Fig. 1 when the energy is near the upper edge of strip 1. This is illustrated in Fig. 2 where we have indicated, schematically,

the contributions to the total NN channel discontinuity $[\mathrm{Im}h_l(T)]$ coming from strips 1 and 2. Since we cannot determine exactly how these strips are contributing, we have made the approximation that

$$\begin{aligned}\mathrm{Im}U(T)&=\mathrm{Im}h(T), \quad 0<T<T_1\\ &=0, \qquad\qquad T>T_1.\end{aligned} \tag{2.17}$$

We realize the crudity of this approximation, but we hope that an appropriate choice of T_1 will result in "reasonable" approximations to $U(T)$. In this paper we consider only $T_1=400$ MeV, for two reasons. First, 400 MeV seems reasonable if we associate $U(T)$ with elastic unitarity in the NN channel, recognizing that the first inelastic channel ($N+N\rightarrow N+N+\pi$) opens up at about 290 MeV and is found to be of little importance below 400 MeV. Second, our determination of $U(T)$ is from experiment (the right-hand cut is always $\mathrm{Im}h^{\mathrm{exp}}$), and "reliable" determinations of p-p partial wave amplitudes extend at present only to about 400 MeV.[1]

We plan, subsequently, to investigate the T_1 dependence of $U(T)$ by making some educated guesses about experiment above 400 MeV and extending our calculations to larger values of T_1. In the meantime, we present the following argument in support of a weak T_1 dependence for the pole parameter values we have obtained. If l is "large," approximation A can be shown to be roughly of the form

$$\mathrm{Im}U_l(T)\sim T^l\int_0^{T_1}\frac{\mathrm{Im}h_l(T')}{T'^l(T'-T)}f(T')dT', \tag{2.18}$$

where $f(T')$ is a slowly varying function of T'. The $(T')^{-l}$ weighting of the integrand in Eq. (2.18) then means that $\mathrm{Im}U_l(T)$ is even less sensitive than $f(T)$ to the upper limit T_1. The argument is, of course, considerably stronger for higher partial waves (large l) than for p waves ($l=1$). It is also only valid for $T\ll T_1$. But for $T\simeq T_1$, our whole approximation scheme breaks down.

III. PROCEDURE AND EXPERIMENTAL INPUT

Phenomenological fits to the p-p scattering data were obtained by adjusting the model pole parameters so that the projected partial-wave scattering amplitudes gave a "best" fit to the p-p scattering data in a least-squares sense. Instead of using the (p,p) data directly, we found it more convenient to work with the reduced matrix representation (RMR) of the data. A detailed discussion of this procedure is available in Ref. 1. (We will refer to Ref. 1 as paper AM.) The RMR is used to calculate the goodness-of-fit parameter, χ^2, for the scattering amplitudes predicted by the model. Actually, our approximations predict the real part of the scattering amplitude $\mathrm{Re}h$, where

$$h=B+U, \tag{3.1}$$

and where h is related to the nuclear "bar" phase shifts[7] by

$$\begin{aligned}h_J&=(E/2ik)(e^{2i\delta_J}-1),\\ &\qquad\text{singlet amplitude},\\ h_{JJ}&=(E/2ik)(e^{2i\delta_{JJ}}-1),\\ &\qquad\text{triplet uncoupled amplitude},\\ h_{J,J\pm1}&=(E/2ik)(\cos2\epsilon_J e^{2i\delta_{J,J\pm1}}-1),\\ &\qquad\text{triplet coupled amplitude},\\ h^J&=(E/2ik)\sin2\epsilon_J e^{i(\delta_{J,J\pm1}+\delta_{J,J-1})},\\ &\qquad\text{coupling amplitude},\end{aligned} \tag{3.2}$$

with $E/k=(1+2M/T)^{1/2}$; J is the angular momentum and M is the nucleon mass. $U(T)$ was calculated from the energy-dependent analysis of Arndt and MacGregor.[1] The p-p data are represented at six energies ($T_{\mathrm{lab}}=25$, 50, 95, 142, 210, and 330 MeV) by the results of single-energy phase-shift analyses, as embodied in the RMR. The RMR elements are essentially the second-order coefficients of a Taylor expansion for χ^2 around the minimum position (δ^0). Since, at the solution, the gradient $(\partial\chi^2/\partial\delta)|_{\delta^0}$ vanishes, we expect that all of the local dependence of χ^2 on the phase shifts is contained in the RMR. In fact, we find that the RMR is a valid (giving χ^2 to within 10% of its actual value) representation of the data even for variations in the phase shifts which result in χ^2 increases of 1000 or more.

Using the RMR to obtain χ^2, we have in a matrix notation,

$$\chi^2\approx\chi^2_{\mathrm{basic}}+\sum_{i=1}^{6}(\delta^i-\delta_0{}^i)^T\alpha^i(\delta^i-\delta_0{}^i), \tag{3.3}$$

where $(\ )^T$ means transpose, and where χ^2_{basic} is the sum of χ^2 values obtained at each energy (25, 50, 95, 142, 210, and 330 MeV) in the phase-shift analyses of AM and equals 259; δ^i is the phase shifts at energy T_i as given by the pole model parameters, $\delta_0{}^i$ is the phase shift vector at minimum χ^2, and energy T_i as given in AM.

$$\alpha_{jk}{}^i=\frac{1}{2}\frac{\partial\chi^2}{\partial\delta_j{}^i\partial\delta_k{}^i}\bigg|_{\delta^i=\delta_0{}^i},$$

where α is the reduced second-derivative matrix defined in AM; $\delta_j{}^i$ is the jth component of δ^i. We will use a shorthand notation, where the sum over energies is implied but not denoted. Equation (3.3) can be written as

$$\Delta\chi^2\sim\Delta\delta(p)^T\alpha\Delta\delta(p),$$

with

$$\begin{aligned}\Delta\delta(p)&=\delta(p)-\delta_0,\\ \Delta\chi^2&=\chi^2-\chi^2_{\mathrm{basic}};\end{aligned} \tag{3.4}$$

[7] M. H. MacGregor, M. J. Moravcsik, and H. P. Stapp, Phys. Rev. 114, 880 (1959).

p is the parameters of our model (i.e., coupling constants and masses).

The χ^2 hypersurface given by Eq. (3.4) still contains a dependence on the $^1S_0$ component of the phase-shift vector. Since our model does not give reliable values for this phase shift, we will work with the reduced hypersurface, $\Delta\chi_r^2(\delta)$, which is obtained by minimizing $\Delta\chi^2$ with respect to the $^1S_0$ phase shift at each energy. This is achieved by singling out the row $(\Delta S)^T$ and column ΔS of α which correspond to the $^1S_0$ phase, and then rewriting Eq. (3.4) as

$$\Delta\chi^2=(\Delta\delta'^T,\Delta S^T)\left(\begin{array}{c|c}\alpha' & \beta\\ \hline \beta^T & \gamma\end{array}\right)\begin{pmatrix}\Delta\delta'\\ \Delta S\end{pmatrix}. \tag{3.5}$$

Solving for the minimum, $\partial\Delta\chi^2/\partial\Delta S=0$, we obtain

$$\Delta S_{\min}=-\frac{1}{\gamma}\beta^T\Delta\delta',$$

and

$$\Delta\chi_r^2=\Delta\delta'^T\left(\alpha'-\frac{1}{\gamma}\beta\beta^T\right)\Delta\delta'$$

$$=\Delta\delta'^T(p)\alpha_r\Delta\delta'(p). \tag{3.6}$$

The vector $\Delta\delta'$ appearing in Eq. (3.6) has no $^1S_0$ component, and it is the reduced hypersurface $\Delta\chi_r^2$ which we will attempt to minimize with the parameters p. First, however, we must transform Eq. (3.6) into the space of Reh [the real part of the scattering ampl tudes defined in Eq. (3.2)]. We will denote Reh, forisimplicity, as a vector h. Then

$$\Delta\delta=\eta\Delta h, \tag{3.7}$$

where

$$\eta_{ll'}\equiv\partial\delta_l/\partial h_{l'}$$

can be solved for from Eq. (3.2). This expression for $\Delta\delta$ can be substituted into (3.6) to obtain an expression for the χ^2 hypersurface in h space:

$$\Delta\chi_r^2=\Delta h^T\eta^T\alpha_r\eta\Delta h=\Delta h^T\alpha_r'\Delta h, \tag{3.8}$$

with

$$\Delta h=h(p)-h(\delta_0)=B(p)+U(\delta_0)-h(\delta_0).$$

Part of our general search procedure will be to linearize B in the particle-exchange parameters (p) which we are determining

$$B(p+\Delta p)=B(p)+\sigma\Delta p, \tag{3.9}$$

with

$$\sigma_{ln}=\left.\frac{\partial B_l}{\partial p_n}\right|_p.$$

Substituting into (3.8) we obtain

$$\Delta\chi_r^2=[\Delta h^T(p)+\Delta p^T\sigma^T]\alpha_r'(\Delta h(p)+\sigma\Delta p)$$
$$=\Delta h^T(p)\alpha_r'\Delta h(p)+2\Delta p^T\sigma^T\alpha_r'\Delta h(p)$$
$$+\Delta p^T\sigma^T\alpha_r'\sigma\Delta p. \tag{3.10}$$

The solution $(\Delta p_{\min})$ to Eq. (3.10) is

$$\Delta p_{\min}=-(\sigma^T\alpha_r'\sigma)^{-1}\sigma^T\alpha_r'\Delta h(p). \tag{3.11}$$

Equation (3.11) is iterated until a solution is achieved $(\Delta p_{\min}\to 0)$.

The number of data represented in our analyses is 363; consequently the statistically acceptable value of χ^2 (the goodness-of-fit parameter) should be around that number since the number of model parameters is small. We emphasize, however, that any rigorous statistical interpretation of χ^2 is unwarranted, when one considers the crudity of our model. We shall use it only as a relative measure of the success of various approximations, but it will be shown that our "best" approximations yield a χ^2 which is nearly statistically acceptable.

IV. RESULTS AND CONCLUSIONS

It is obvious that the approximations we have thus far described are for a low-energy theory and, consequently, will begin to fail above some energy. We expect that the "potential" term $B(T)$ will fail at energies where the exchange of heavier systems (greater than M_ω) begins to manifest itself in the lowest $(l=1)$ states treated by the model. Also, the unitarity corrections are singular if we attempt to evaluate them at energies near the energy of the strip parameter T_1 (400 MeV). Because of these considerations, we decided that the approximations should be studied as a function of "minimum-impact parameter" $a_{\min}$. We first define the impact parameter $a_l(k)$ for the lth partial wave at c.m. momentum k as

$$a_l(k)=[l(l+1)]^{1/2}/k, \quad \text{(expressed in fermis)},$$
$$k=\text{c.m. momentum}=(\tfrac{1}{2}MT)^{1/2}. \tag{4.1}$$

In defining a minimum-impact parameter $a_{\min}$ for the model we simply mean that for all energies such that

$$a_l(k)>a_{\min}, \tag{4.2}$$

phase shifts are determined by the model. For those energies where the above relationship does not hold, the phase shift is determined as a free, phenomenological, parameter. This is accomplished by using the same reduction procedure as described above for the phenomenological $^1S_0$ phase shift [Eqs. (3.5) and (3.6)]. It is encouraging to note that the phenomenologically determined phases from the reduction procedure remain within a few standard deviations ($\Delta\delta$ given in Table I) of the "experimental" (δ of Table I) values. Ideally we would expect that a "best" determination of the coupling parameters would be obtained from a study of the long-range part of the interaction, since the *theoretical* uncertainties of our model are smallest there. Unfortunately, the *experimental* uncertainties resulting from partial-wave analyses are largest for large $a_{\min}$. It is our prescription, therefore, to

TABLE I. Approximations to $U(T)$ multiplied by $(180/\pi)(k/E)$ to read in degrees. $T_1=400$ MeV.

Phase	T_{lab} (MeV)	δ[a]	$\Delta\delta$[a]	$A(9\mu^2)$[b]	$A(20\mu^2)$[b]	$A(40\mu^2)$[b]	$A(\infty)$[b]	$B(0)$[b]	$B(4)$[b]
$^3P_0$	25	7.22	1.38	0.77	0.66	0.61	0.55	0.69	0.6
	50	12.48	0.87	−0.28	−0.53	−0.65	−0.79	−0.52	−0.7
	95	13.26	2.69	−2.15	−2.57	−2.82	−3.15	−2.6	−3.0
	142	6.22	0.61	−1.91	−2.44	−2.81	−3.36	−2.5	−3.0
	210	−1.	0.6	−0.64	−1.25	−1.75	−2.61	−1.3	−2.0
	330	−12.9	1.5	1.06	0.41	−0.22	−1.60	0.26	−0.6
$^3P_1$	25	−3.25	0.55	0.76	0.53	0.44	0.35	0.59	0.43
	50	−7.88	0.36	1.64	1.16	0.93	0.68	1.23	0.9
	95	−12.80	0.72	2.8	1.97	1.49	0.90	2.01	1.38
	142	−16.60	0.43	3.2	2.15	1.45	0.47	2.11	1.23
	210	−21.80	0.61	2.36	1.13	0.20	−1.34	0.95	−0.2
	330	−28.9	1.12	−3.93	−5.24	−6.42	−8.90	−5.7	−7.15
$^3P_2$	25	1.91	0.28	0.47	0.35	0.30	0.25	0.38	0.3
	50	6.09	0.23	1.07	0.82	0.70	0.57	0.87	0.69
	95	9.88	0.56	1.53	1.1	0.86	0.55	1.13	0.8
	142	13.73	0.21	1.18	0.64	0.28	−0.23	0.61	0.15
	210	15.84	0.27	−0.07	−0.7	−1.78	−1.98	−0.81	−1.4
	330	16.32	0.64	−2.96	−3.63	−4.24	−5.5	−3.9	−4.7
$^1D_2$	25	0.69	0.17	0.019	0.012	0.01	0.007	0.02	0.02
	50	2.2	0.28	0.065	0.04	0.025	0.013	0.06	0.06
	95	3.52	0.31	0.15	0.07	0.026	−0.026	0.13	0.11
	142	5.32	0.25	0.19	0.05	−0.036	−0.16	0.14	0.11
	210	7.05	0.33	0.12	−0.09	−0.26	−0.54	0.03	−0.02
	330	9.03	0.69	−0.59	−0.88	−1.17	−1.87	−0.74	−0.82
ϵ_2	25	−0.85	0.35	−0.04	−0.02	−0.02	−0.01	−0.04	−0.03
	50	−2.3	0.36	−0.07	−0.02	−0.002	0.02	−0.06	−0.06
	95	−2.62	0.47	0.03	0.16	0.24	0.35	0.06	0.08
	142	−2.7	0.15	0.23	0.47	0.63	0.88	0.31	0.35
	210	−2.8	0.19	0.50	0.86	1.16	1.73	0.64	0.72
	330	−3.04	0.49	0.95	1.44	1.98	3.35	1.2	1.31
$^3F_2$	25	−0.18	0.41	0	−0.003	−0.004	−0.005	0	0
	50	0.61	0.37	−0.03	−0.05	−0.05	−0.63	−0.02	−0.03
	95	−0.01	0.98	−0.14	−0.22	−0.28	−0.36	−0.13	−0.15
	142	0.57	0.41	−0.26	−0.44	−0.60	−0.89	−0.25	−0.30
	210	1.58	0.34	−0.38	−0.74	−1.14	−2.07	−0.37	−0.47
	330	0.70	0.68	−0.51	−1.18	−2.17	−5.53	−0.54	−0.72
$^3F_3$	25	−0.23		0.001	0	0	0	0	0.001
	50	−0.48	0.41	0.004	0.001	0	0	0.005	0.003
	95	−0.69	1.07	0.002	−0.01	−0.02	−0.03	0.004	−0.001
	142	−1.73	0.24	−0.01	−0.05	−0.069	−0.11	−0.012	−0.02
	210	−2.61	0.22	−0.05	−0.12	−0.18	−0.3	−0.06	−0.08
	330	−3.22	0.63	−0.17	−0.28	−0.43	−0.88	−0.18	−0.22
$^3F_4$	25	0.015		0	0	0	0	0	0
	50	0.13	0.21	0	0	0.001	0	0.003	0.002
	95	0.40	0.28	0.01	0.006	0.003	0	0.012	0.009
	142	0.86	0.21	0.02	0.008	0.001	−0.01	0.021	0.016
	210	2.28	0.20	0.024	−0.001	−0.021	−0.05	0.022	0.013
	330	2.97	0.42	−0.06	−0.11	−0.15	−0.28	−0.07	−0.08
ϵ_4	25	−0.048		0	0	0	0	0	0
	50	−0.19		0	0	0	0	0	0
	95	−0.49		0	0	0.002	0.004	−0.003	−0.002
	142	−0.58	0.08	0	0.01	0.015	0.024	−0.001	0
	210	−0.97	0.1	0.016	0.04	0.058	0.103	0.013	0.016
	330	−0.77	0.30	0.07	0.12	0.19	0.444	0.07	0.075
$^1G_4$	25	0.039		0	0	0	0	0	0
	50	0.14		0	0	0	0	0	0
	95	0.34		0	−0.001	−0.002	−0.003	0.001	0.001
	142	0.59	0.17	0	−0.006	−0.01	−0.016	0.001	0
	210	1.06	0.15	−0.006	−0.02	−0.033	−0.06	−0.004	−0.006
	330	1.51	0.34	−0.03	−0.07	−0.11	−0.28	−0.03	−0.036
$^3H_4$	25	0.004		0	0	0	0	0	0
	50	0.025		0	0	−0.001	0	0	0
	95	0.095		−0.004	−0.01	−0.01	−0.01	−0.002	−0.003
	142	−0.26	0.21	−0.01	−0.03	−0.046	−0.08	−0.008	−0.01
	210	0.35	0.36	−0.04	−0.09	−0.17	−0.40	−0.02	−0.03
	330	1.49	0.42	−0.08	−0.25	−0.62	−2.6	−0.06	−0.07

[a] Phases (δ) and "errors" ($\Delta\delta$) in degrees from AM [Ref. (1)]. Phases treated as one-pion-exchange contributions by AM have no errors quoted.
[b] These approximations are defined in the text.

study the various models [different $U(T)$] as a function of $a_{\min}$, to see the effect both on χ^2 and on the pole parameters.

Determinations of $U(T)$ resulting from a number of different approximations are tabulated for comparison in Table I. The first observation to be found in Table I is the smallness, in general, of the unitarity term when compared to the amplitude to which it applies. Notable exceptions to this behavior are ϵ_2 and ${}^3F_2$, where $U(T)$ is increased because of coupling to lower (smaller l) and much larger amplitudes. For these coupled states we have

$$\mathrm{Im}h_{j,j\pm1}=\frac{k}{E}(\sin^2\epsilon+\sin^2\delta_\pm). \tag{4.3}$$

At threshold,

$$\epsilon\propto T^{j+1/2},\quad \delta_\pm\propto T^{j+(1/2)\pm1}. \tag{4.4}$$

Hence we expect the low-energy S-channel cut for the amplitude $h_{l=j+1}$ to be largely determined by ϵ. This is, in fact, the observed case for the p-p system. In the low-energy (0–200-MeV) region, ϵ_2 is 2–3 times as large as ${}^3F_2$. This situation also manifests itself, though not so noticeably, in the $j=4$ amplitude, where ${}^3H_4$ couples to ϵ_4 to produce a relatively large $U(T)$.

The next observation we would like to make about Table I is the strong similarity between various approximations to $U(T)$. Since the only way in which these approximations differ is the discontinuity across the left-hand cut [$\mathrm{Im}h(T)$ for $-\infty<T<-T_L$], the similarity in $U(T)$ suggests that our approximations may be insensitive to the precise structure of the left-hand cut. To further illustrate this point, we direct the reader's attention to those entries in Table I corresponding to [$(A)\bar{t}=20\mu^2$], [$(B)j_k=0$], and [$(B)j_k=4$]. The left-hand discontinuities associated with these three approximations are depicted in Fig. 3. These three different approximations give quite similar contributions in the energy range of interest (the near right-hand cut), despite radically different left-hand cut structures.

Finally, it should be noted in Table I that as $T\rightarrow T_1$, the corrections $U(T)$ become very large and probably unreliable.

It is relevant to point out here that the two approximations studied, A and B, are derived from essentially different philosophies. In approximation A, the left-hand cut structure is a consequence of the approximations described in IIB, while in approximation B, a specific structure is assumed with just enough flexibility to satisfy the conditions (2.3). In either case, $U(T)$ must be interpreted as a phenomenological representation of that part of the amplitude required by s-channel unitarity. The reason for its introduction is to make our determination of the potential more reliable. With this purpose in mind, we first deduce the "optimum" value of $\bar{t}$ to be used in approximation A. This is accomplished in Table II, where we have depicted $\chi^2(\bar{t},a_{\min})$. It is

TABLE II. Determination of χ^2 for $U=A(\bar{t})$ from 4-pole fit to $\mathrm{Re}h^{\exp}(T)-U(T)$.

$a_{\min}$	$\delta(T_{\mathrm{lab}})$[a]	$9\mu^2$	$20\mu^2$	$40\mu^2$	$60\mu^2$	$100\mu^2$	∞
0.7	$P(330)$	1185	918	808	796	824	1013
0.89	$P(210)$	837	612	522	514	540	715
1.	$P(140)$	764	547	460	451	475	638
1.2	$D(330)$	618	468	413	416	447	614
1.3	$P(95)$	612	466	409	410	441	608
1.5	$D(210)$	476	394	363	384	409	580
1.7	$F(330)$	432	376	360	382	404	562
1.85	$D(140)$	349	329	324	333	355	473
2.2	$G(330)$	323	314	313	320	340	447
2.75	$H(330)$	284	285	284	287	297	346

[a] Insufficient data prevented determination.

clear from the results of this study that the "optimum" is around $\bar{t}=40\mu^2$ (noting that for any $a_{\min}$, χ^2 is smallest for $\bar{t}=40\mu^2$) and that there is a rather broad range of acceptable $\bar{t}$ values. We select $\bar{t}=40\mu^2$ to use for comparison with other approximations [$U=0$, and $U=B$ $(j_1=0)$], and also for comparison to the "extreme" values $\bar{t}=9\mu^2$ and $\bar{t}=\infty$.

Once the unitarity corrections have been investigated, we can proceed to the pole-fitting calculations. Our "potential" should represent the low angular-momentum states in the crossed $(N\bar{N})$ reaction. Thus we choose a $\pi(S=0,\ J=0,\ I=1)$, a $\rho(J=S=I=1)$, and an $\omega(J=1,\ S=1,\ I=0)$ as exchanges embodied in the potential. These particles represent three of the four $N\bar{N}$ S waves. The fourth $(J=0,\ I=0)$ S wave could be represented by an η. However, since the η contributes like the π in PP states, we were unable to distinguish its contribution from that of the π. Therefore, it was not included in our description of the potential. The vector particles (ρ,ω) represent an admixture of S and D waves in the $I=1$ and $I=0$ states, respectively. Normally they would contribute identically to the p-p scattering states. However, we will use the results of electromagnetic-form-factor studies to fix the (f/g) ratio of the ρ at 4, and of the ω at 0. Under these circumstances the ρ and ω contributions are distinct. Finally, we invoke a σ meson $(I=0,\ J^P=0^+)$ to represent an exchange in the $N\bar{N}$, $I=0$, ${}^3P_0$ state. The need for such an exchange term is described in Ref. 5. We will later discuss the fact that, on the basis of NN scattering data alone, we cannot deduce the existence of a σ "particle," but we use the σ as a convenient representation of any exchange in the $N\bar{N}$ state having the quantum numbers of the σ. Our determined (searched) parameters are g_π^2, g_σ^2, g_ω^2, g_ρ^2, and M_σ. We will take as fixed the M_π, M_ω, M_ρ, $(f/g)_\omega$, and $(f/g)_\rho$ parameters.

The results of our analyses are summarized in Table III, where we have tabulated our determinations for five different approximations to $U(T)$ as a function of the minimum-impact parameter $a_{\min}$. In addition, at the bottom of Table III we have included the analyses where only states with $l\geq2$ were used to determine the model parameters. The first part of Table III gives the goodness-of-fit parameter χ^2 while the remainder of

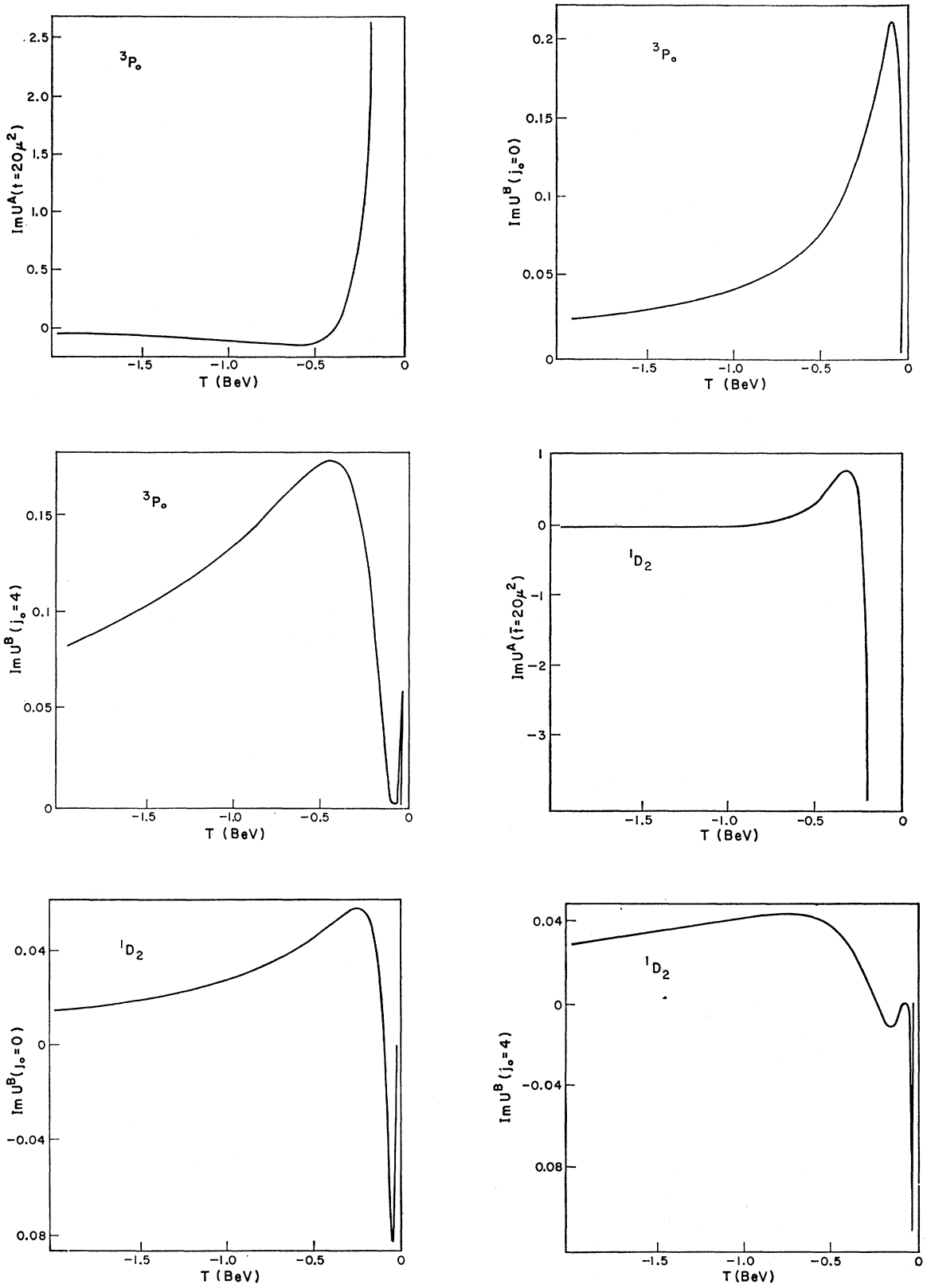

FIG. 3. Left-hand discontinuities in $U(T)$ for the following approximations to $U(T)$: $U^A(t=20\mu^2)$, $U^B(j_0=0)$, $U^B(j_0=4)$.

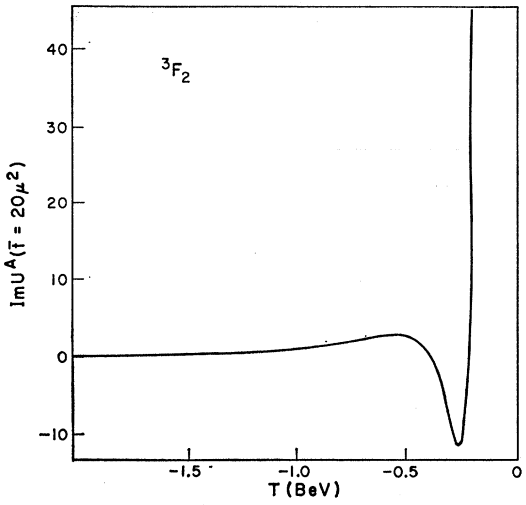

FIG. 3. (*continued*).

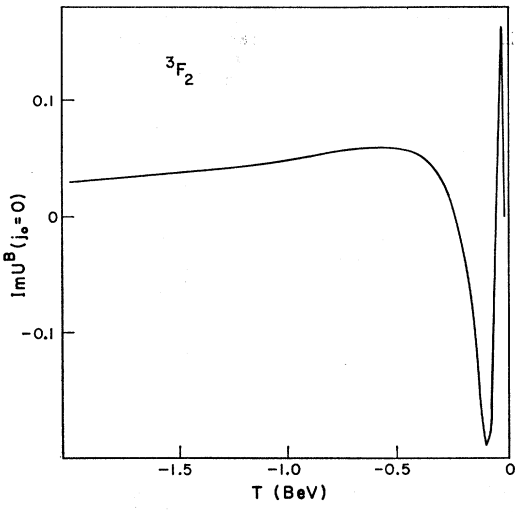

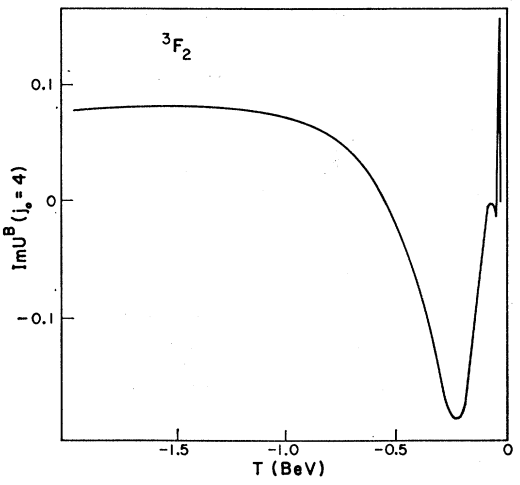

the table gives the corresponding values of the pole parameters with errors. The errors have the usual interpretation in terms of an error matrix. That is, if any parameter p were changed by an amount Δp (the error), and the remaining parameters were allowed to "adjust," the resulting increase in χ^2 would be one. The column next to $a_{\min}$ indicates the angular-momentum state and lab energy which corresponds to $a_{\min}$.

The first consequence of Table III which is noteworthy is that the case $U=A(40\mu^2)$ is strongly preferred (in terms of χ^2 for any value of $a_{\min}$) over the other approximations considered. If we were to select a model solely on its ability to fit the data, our choice would be $U=A(40\mu^2)$ with $1\ F<a_{\min}<2$ F.

Now consider the pole-coupling-constant values that correspond to the χ^2 values (Table III). As indicated previously, the errors on parameters increase with $a_{\min}$, indicating an increasing loss of experimental information. The problem, then, is to select the pole parameters from a region of $a_{\min}$ where the theoretical uncertainties are smallest (larger $a_{\min}$), but where we still have sufficient experimental information to make the determination. We can even look for a range of impact parameters over which our determinations are "stable." We can see from Table III that the determinations are most stable for the case $U=A(\bar{t}=40\mu^2)$ in the range $1\ F<a_{\min}<2$ F. The determinations corresponding to $U=A(\bar{t}=40\mu^2)$ are plotted in Fig. 4. This is precisely the approximation which yields a minimum χ^2, and hence we take the corresponding pole parameters to be our "best" values. These are the parameters given in the abstract. The range of parameter values achieved for all approximations to $U(T)$ is small, which suggests that the uncorrected pole terms, $U(T)=0$, account for a considerable part of the "gross structure" of the p-p scattering amplitude. This matter is discussed in detail by Bryan and Arndt.[5] As far as the corrections are concerned, any of the approximations studied here are capable of yielding a qualitative fit to the data. The introduction of our approximations to $U(T)$ results in semiquantitative fits which we feel somewhat enhance the reliability of our pole determinations. It is interesting to note that g_π^2, which was treated as a free parameter, turns out to be quite close to, and consistent with, the generally accepted value of 14.8.[8] Our "best" determination of g_π^2 is around 14 ± 0.2 as deduced from the results in Table III with $U=A(40\mu^2)$ and with $1\ F<a_{\min}<1.7$ F.

To illustrate, graphically, the type of fit we achieve, we have plotted in Fig. 5 the results of our best [$U=A(\bar{t}=40\mu^2)$, $a_{\min}=1.3$ F] determination to the phase shifts ($1\leq l\leq 4$). These pictures illustrate, roughly, the

[8] V. K. Samaranayake and W. S. Woolcock, Phys. Rev. Letters **15**, 936 (1965); J. Hamilton and W. S. Woolcock, Rev. Mod. Phys. **35**, 737 (1963). Reference 1 also contains a determination of g_π^2.

TABLE III. Determination of χ^2 and of the searched pole parameters as a function of $a_{\min}$ and for various approximations to $U(T)$. $a_{\min}$ is the "minimum-impact parameter" defined in 4.2. $\delta(T_{\text{lab}})$ is the phase shift and energy (in MeV) corresponding to $a_{\min}$. The phases determined by model parameters in these analyses include $\delta(T_{\text{lab}})$ and exclude all $\delta(T_{\text{lab}})$ appearing in preceding rows of the table. The last row of this table gives determinations where all phases, excluding P waves, were fitted at all energies.

$a_{\min}$	$\delta(T_{\text{lab}})$	$U=0$	$A(40\mu^2)$	$A(9\mu^2)$	$A(\infty)$	$B(0)$
			Determination of χ^2			
0.7	$P(330)$	1280	808	1185	1013	1063
0.89	$P(210)$	1047	522	837	715	748
1.	$P(140)$	897	460	764	638	685
1.2	$D(330)$	783	413	618	614	576
1.3	$P(95)$	740	409	612	608	569
1.5	$D(210)$	662	363	476	580	460
1.7	$F(330)$	514	360	432	562	425
1.85	$D(140)$	421	324	349	473	351
2.2	$G(330)$	361	313	323	447	327
2.75	$H(330)$	286	284	284	346	284
All $l>1$ All T_{lab}		418	329	371	463	372
			Determination of g_π^2			
0.7	$P(330)$	12.5±0.14	14.2±0.14	14.4±0.14	14. ±0.14	14.3±0.14
0.89	$P(210)$	12.8±0.14	14.2±0.15	14.4±0.14	14.2±0.14	14.3±0.15
1.	$P(140)$	13.1±0.17	14.0±0.17	14.2±0.17	13.9±0.17	14.1±0.17
1.2	$D(330)$	12.7±0.17	14.0±0.17	14. ±0.17	13.9±0.18	13.9±0.17
1.3	$P(95)$	13.3±0.20	13.9±0.2	14.3±0.2	13.7±0.19	13.9±0.17
1.5	$D(210)$	13.1±0.20	13.7±0.2	13.9±0.2	13.6±0.2	13.8±0.2
1.7	$F(330)$	14.1±0.24	13.9±0.24	14.4±0.2	13.5±0.23	14.3±0.24
1.85	$D(140)$	13.3±0.29	13.4±0.29	13.2±0.29	13.7±0.2	13.3±0.3
2.2	$G(330)$	13.7±0.41	13 ±0.42	13.2±0.41	13.2±0.42	13.2±0.4
2.75	$H(330)$	10.9±0.81	11 ±0.81	11 ±0.8	a	11 ±0.8
All $l>1$ All T_{lab}		13.3±0.35	13.6±0.33	13.1±0.35	13.4±0.3	13.2±0.4
			Determination of g_σ^2			
0.7	$P(330)$	2.5± 0.1	2.8± 0.1	3.1± 0.1	2.8±0.1	3.1± 0.1
0.89	$P(210)$	2.8± 0.1	3.2± 0.1	3.4± 0.1	3.1±0.1	3.4± 0.1
1.	$P(140)$	2.9± 0.1	3.1± 0.1	3. ± 0.1	3.3±0.1	3.1± 0.1
1.2	$D(330)$	4.4± 0.3	2.9± 0.3	3.3± 0.3	2.5±0.3	3.4± 0.3
1.3	$P(95)$	4.2± 0.3	2.9± 0.3	3.3± 0.3	2.5±0.3	3.4± 0.3
1.5	$D(210)$	6.4± 0.6	2.8± 0.4	4 ± 0.5	2 ±0.3	4 ± 0.5
1.7	$F(330)$	5.9± 0.7	2.9± 0.4	3.8± 0.5	2 ±0.3	3.9± 0.5
1.85	$D(140)$	21 ± 3	4 ± 1.1	11 ± 2	0.9±0.4	11 ± 2
2.2	$G(330)$	9 ± 3	2.3± 1.3	5 ± 2	0.7±0.5	5.4± 2
2.75	$H(330)$	124 ±103	53 ±77	87 ±89	a	91 ±90
All $l>1$ All T_{lab}		12.2± 4	3.5± 1.3	11.6± 4	1.7±0.6	12.6± 0.4
			Determination of g_ω^2			
0.7	$P(330)$	3.3± 0.1	0.93± 0.1	1.5± 0.1	0.33±0.1	1.2± 0.1
0.89	$P(210)$	4 ± 0.1	2.1 ± 0.1	2.9± 0.1	1.4 ±0.1	2.6± 0.1
1.	$P(140)$	4.2± 0.3	3.1 ± 0.3	3.4± 0.3	2.9 ±0.3	3.2± 0.3
1.2	$D(330)$	7.8± 0.6	3.9 ± 0.6	5.1± 0.6	3.1 ±0.6	4.8± 0.6
1.3	$P(95)$	5.2± 0.7	4 ± 0.7	4.2± 0.7	3.7 ±0.7	3.9± 0.7
1.5	$D(210)$	6.4± 1	5.8 ± 1	7 ± 1	5 ±1	6.5± 1
1.7	$F(330)$	2.3± 1.1	4.9 ± 1.1	5 ± 1.1	5.2 ±1.1	4.5± 1.1
1.85	$D(140)$	20 ± 2.6	10 ± 2.7	18 ± 2.6	2 ±2.4	18 ± 2.6
2.2	$G(330)$	1.2± 4.3	0.9 ± 4.4	3.3± 4.4	−2 ±4	2.9± 4.3
2.75	$H(330)$	132 ±55	6.8 ±54	96 ±54	a	101 ±55
All $l>1$ All T_{lab}		19 ± 2.2	5.7 ± 1.8	15 ± 2.2	0.8 ±1.5	15 ± 2.2
			Determination of g_ρ^2			
0.7	$P(330)$	0.9±0.02	1.2 ±0.02	1.2 ±0.02	1.2±0.02	1.2±0.02
0.89	$P(210)$	0.9±0.03	1.13±0.03	1.05±0.03	1.2±0.03	1.1±0.03
1.	$P(140)$	1 ±0.04	1.08±0.04	1.06±0.04	1.1±0.04	1.1±0.04
1.2	$D(330)$	1 ±0.05	1.18±0.05	1.26±0.05	1.1±0.05	1.2±0.05
1.3	$P(95)$	1.3±0.07	1.18±0.07	1.4 ±0.07	1 ±0.07	1.3±0.07
1.5	$D(210)$	1.4±0.08	1.13±0.08	1.3 ±0.08	1 ±0.08	1.3±0.08
1.7	$F(330)$	1.7±0.1	1.24±0.11	1.5 ±0.11	1 ±0.11	1.5±0.11
1.85	$D(140)$	1.2±0.2	1.04±0.17	1.1 ±0.17	1.3±0.18	1 ±0.16
2.2	$G(330)$	2.3±0.4	1.7 ±0.36	2 ±0.4	1.6±0.4	2 ±0.4
2.75	$H(330)$	−12 ±4.5	−11 ±5	−11 ±5	a	−11 ±5
All $l>1$ All T_{lab}		1.6±0.2	1.0 ±0.16	1.2 ±0.2	0.6±0.14	1.1±0.2

TABLE III. (*continued*).

a_{min}	$\delta(T_{lab})$	$U=0$	$A(40\mu^2)$	$A(9\mu^2)$	$A(\infty)$	$B(0)$
			Determination of M_σ			
0.7	$P(330)$	430±3	475±5	493±5	471±5	488±5
0.89	$P(210)$	437±3	474±5	490±5	471±5	486±5
1.	$P(140)$	434±5	464±5	466±6	470±5	467±6
1.2	$D(330)$	462±8	446±10	459±10	431±10	460±10
1.3	$P(95)$	468±9	445±10	461±11	430±10	463±11
1.5	$D(210)$	515±14	433±14	471±14	396±13	472±14
1.7	$F(330)$	519±16	437±14	471±16	400±14	474±16
1.85	$D(140)$	615±17	451±24	544±18	332±30	547±18
2.2	$G(330)$	575±36	430±43	506±37	325±48	517±37
2.75	$H(330)$	647±68	607±113	627±82	a	630±80
All $l>1$		567±31	453±34	567±33	384±30	575±32
All T_{lab}						

[a] Insufficient data prevented determination.

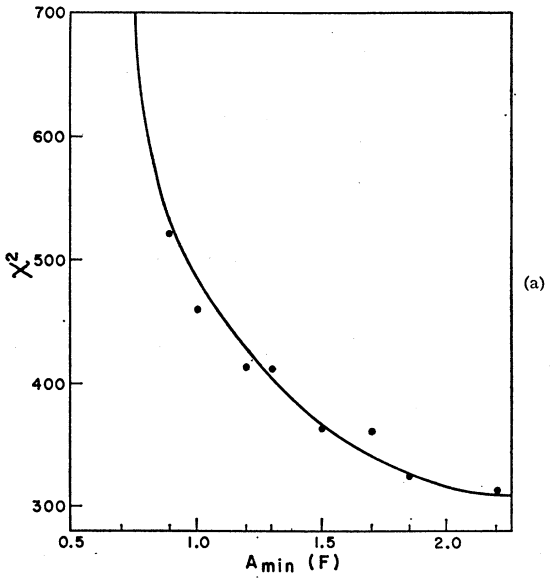

FIG. 4. Determination of pole parameters for $U=A(\bar{l}=40\mu^2)$ as a function of minimum impact parameter, a_{min}.

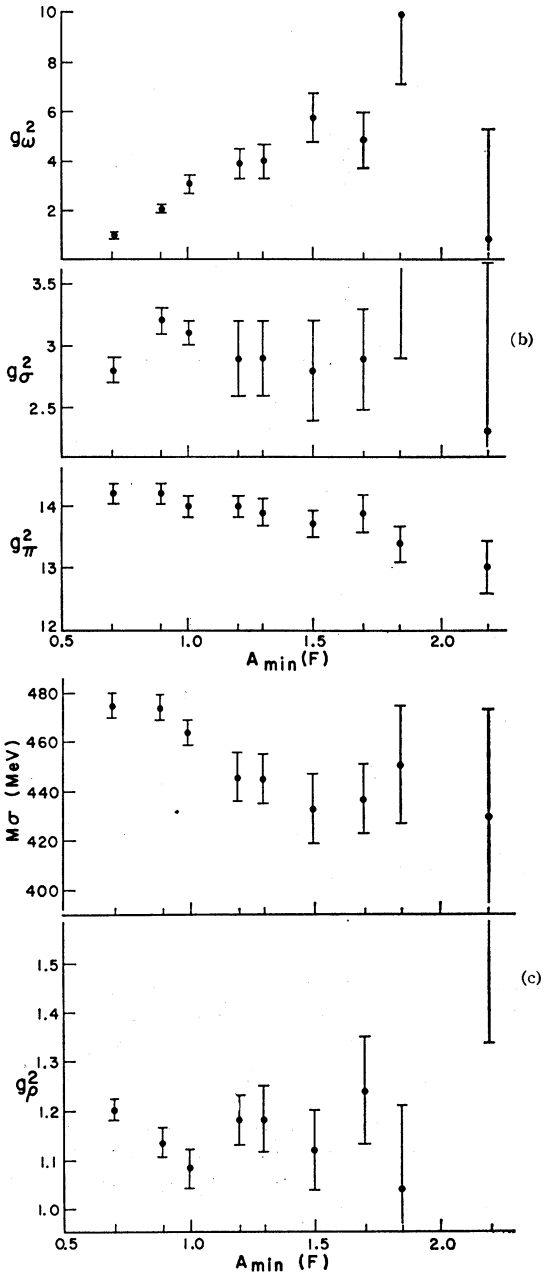

experimental state of the p-p system as well as the degree of success we have achieved in fitting the phase shifts with unitarized poles.

The scalar mass obtained in our "best" determination is high enough (450 MeV) that its effects would not be seen in reactions like K_{e4} decay, where it has been looked for and not found.[9] Durso and Signell[10] have demonstrated the equivalence of a continuum ALV[11]

[9] Birge *et al.*, Phys. Rev. **139**, B1600 (1965).
[10] J. W. Durso and P. Signell, Phys. Rev. **135**, B1057 (1964).
[11] D. Amati, E. Leader, and B. Vitale, Nuovo Cimento **17**, 68 (1960); **18**, 409 (1960); Phys. Rev. **130**, 750 (1963).

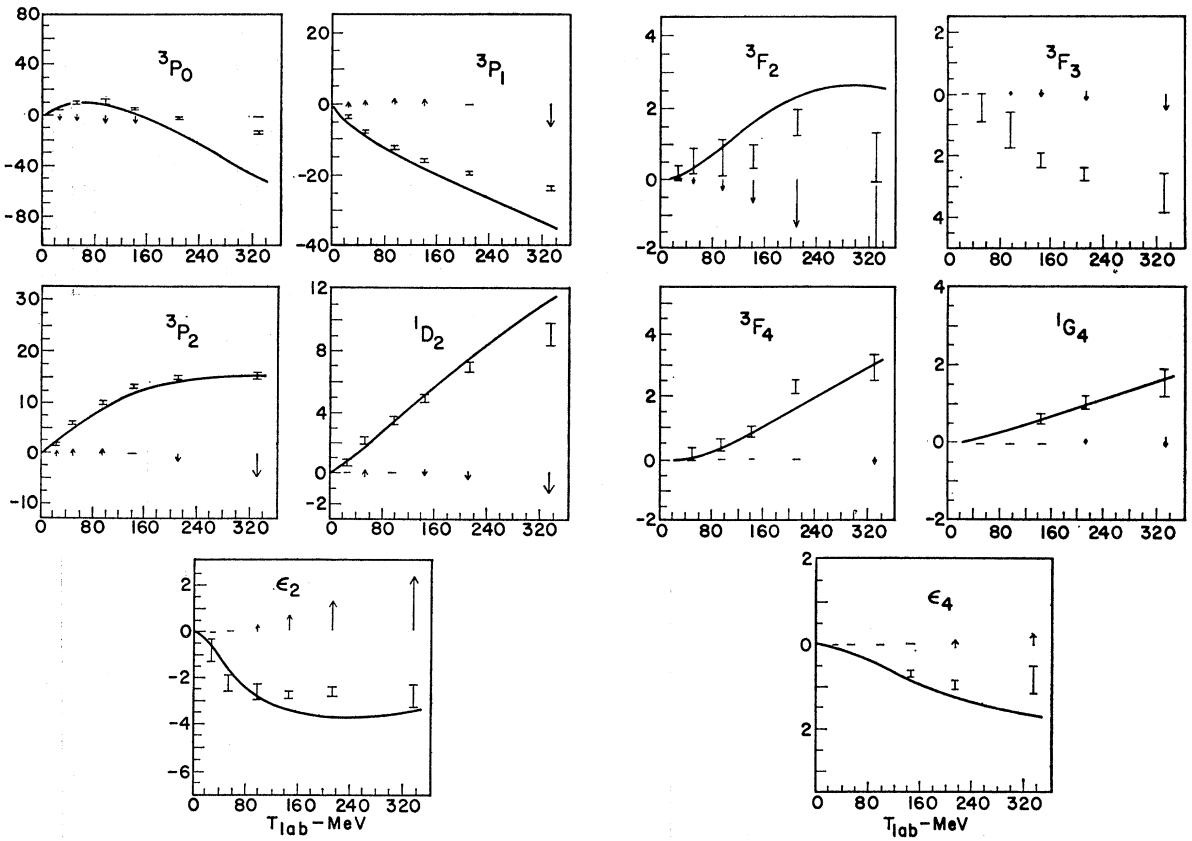

FIG. 5. Four-pole fit to partial-wave amplitudes $l=1$ through $l=4$ with $a_{\min}=1.3$ F and with $U(t)$ given by $U^A(t=40\mu^2)$. The solid curves are the potential $[B(T)]$ for the parameters given in Table III. The arrows indicate the unitarity term $U(T)$ and the "experimental" points (indicated with error bars) are from the analyses of Arndt and MacGregor (Ref. 1). The comparison to be drawn at each energy is between the experimental value and the sum of B and U.

2π S-wave contribution to that of a σ_0 meson of mass $\sim$400 MeV and $g_\sigma^2\sim 4.7$. Evidently, therefore, we cannot claim the existence of a σ "particle" from our analysis, but we do measure the strength of the equivalent effect in that channel that is required to match the observed p-p phase shifts.

In conclusion, we feel that the inclusion of a reasonable approximation to $U(T)$ leads to a significant improvement in the fit to the amplitudes, thereby giving us increased confidence in the particle representation for the potential.

ACKNOWLEDGMENTS

One of us (R.A.A.) is deeply indebted to Professor G. Chew for his encouragement, and for his enlightenment of the subject matter covered herein. We would also like to thank Dr. Elliot Leader and Dr. Michael Moravcsik for stimulating discussions. Finally, to Dr. Sidney Fernbach, as representing the Theoretical Physics Division of the Livermore branch of UCLRL, we wish to express gratitude for the support which made this work possible.

APPENDIX I: THRESHOLD BEHAVIOR OF LEFT-HAND CUT

Here we examine the behavior of the left-hand discontinuity of the NN scattering amplitude as $q_s^2\to-\mu^2$; that is, as we approach the near end of the left cut. The discontinuity is exhibited in Figs. 6 and 7 in the t and q_s^2 complex planes. Expanding the $N\bar{N}\to N\bar{N}$ amplitude in the t channel we obtain

$$A^{(N\bar{N})^2}(t,Z_t)=\sum_l P_l(Z_t)A_l{}^{(N\bar{N})^2}(t)(2l+1),$$

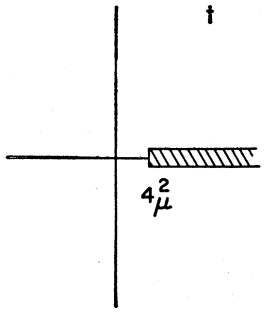

FIG. 6. Near end of left-hand discontinuity of A in t variable.

from which

$$\mathrm{Im}A^{(N\bar{N})^2}(t,Z_t)=\sum_l(2l+1)P_l(Z_t)\,\mathrm{Im}A_l{}^{(N\bar{N})^2}(t).$$

Now for $4\mu^2<t<9\mu^2$ we have the relationship

$$\mathrm{Im}A_l{}^{(N\bar{N})^2}(t)=\frac{q_\pi}{\sqrt{t}}|A_l{}^{\pi\pi\to N\bar{N}}(t)|^2,\quad q_\pi=(t-4\mu^2)^{1/2}$$

as

$$q_\pi\to 0,\quad A_l{}^{\pi\pi\to N\bar{N}}(t)\sim q_\pi{}^l;$$

$$q_\pi=(t-4\mu^2)^{1/2}\to 0,\quad Z_t\sim\frac{S}{q_\pi}.$$

We obtain

$$\mathrm{Im}A=D_t(\text{discontinuity})\sim\sum_l\alpha_l(t-t_0)^{1/2}$$
$$D_t\sim(t-t_0)^{1/2}.$$

If we now decompose this discontinuity into partial waves in the NN channel we obtain (expressing D in terms of q_s^2, z_s),

$$D_l(q_s{}^2)=\int_{-1}^{+1}P_l(Z_s)D_t(q_s{}^2,Z_s)dZ_s,$$

where $Z_s=1+t/2q_s{}^2$. Noting now that $D_t=0$ for $t<4\mu^2$, we have

$$D_t(q_s{}^2,Z_s)=0\quad\text{for}\quad Z_s>1+2\mu^2/q_s{}^2,$$

or

$$D_l(q_s{}^2)\propto\int_{-1}^{1+2\mu^2/q_s{}^2}P_l(Z_s)(t-4\mu^2)^{1/2}dZ_s$$

and

$$D_l\underset{q_s{}^2\to-\mu^2}{\propto}(-1)^l\int_{-1}^{1+2\mu^2/q_s{}^2}(t-4\mu^2)^{1/2}dz_s,$$

from which

$$D_l(q_s{}^2)\underset{q_s{}^2\to-\mu^2}{\propto}(-q_s{}^2-\mu^2)^{3/2},$$

which in terms of $T=2q_s{}^2/M$ and $X=1+2\mu^2/MT$ variables become

$$D_l(T,X)\sim(-T-2\mu^2/M)^{3/2}$$
$$\sim(X+1)^{3/2}$$

as $T\to-2\mu^2/M$ or $X\to-1$.

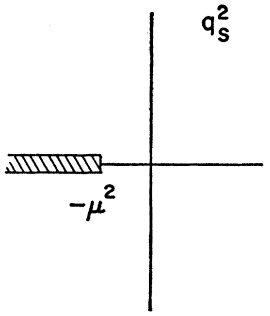

FIG. 7. Near end of left-hand discontinuity of A in $q_s{}^2$ variable.

APPENDIX II: PARTIAL-WAVE PROJECTIONS FOR ONE-BOSON EXCHANGE

T is the lab kinetic energy (MeV). k is the c.m. momentum $=(\frac{1}{2}MT)^{1/2}$. M is the nucleon mass $=938.2$ MeV. ϵ is the c.m. energy of either nucleon $=M(1+T/2M)^{1/2}$. G equals $\frac{1}{4}g^2$. μ is the mass of exchanged particle.

$$x_0=1+\mu^2/2k^2=1+\mu^2/MT.$$
$$a=[k(\epsilon+M)]^2.$$

B_J is the projection on singlet state. B_{JJ} is the projection on triplet uncoupled state. $B_{J,J-1}$ is the projection on triplet state $l=J-1$. $B_{J,J+1}$ is the projection on triplet state $l=J+1$. B^J is the projection on coupling state.

Note: $I=0$, NN phases are multiplied by a factor (-3) if the exchanged particle has isospin $=1$.

A. Pseudoscalar ($J^P=0^-$) Exchange

$$B_J=G[(x_0-1)Q_J(x_0)-\delta_{J,0}],$$
$$B_{JJ}=G[(x_0+1)Q_J(x_0)-Q_{J+1}(x_0)-Q_{J-1}(x_0)],$$
$$B_{J,J-1}=-(G/(2J+1))[Q_J(x_0)-Q_{J-1}(x_0)],$$
$$B_{J,J+1}=-(G/(2J+1))[Q_{J+1}(x_0)-Q_J(x_0)],$$
$$B^J=-G[J(J+1)]^{1/2}/(2J+1)\times[Q_{J+1}(x_0)+Q_{J-1}(x_0)-2Q_J(x_0)].$$

B. Scalar ($J^P=0^+$) Exchange

$$B_J=(G/2a)(1+a^2-2ax_0)Q_J(x_0),$$

$$B_{JJ}=G\frac{(1+a^2+2ax_0)}{2a}Q_J(x_0)-Q_{J+1}(x_0)-Q_{J-1}(x_0),$$

$$B_{J,J-1}=\frac{G}{(2J+1)}\left\{\frac{(1+a^2+2J(1-a^2))}{2a}Q_{J-1}(x_0)+[2J(ax_0-1)-1]Q_J(x_0)\right\},$$

$$B_{J,J+1}=\frac{G}{(2J+1)}\left\{\frac{[1-3a^2+2J(1-a^2)]}{2a}Q_{J+1}(x_0)+[2J(ax_0-1)+2ax_0-1]Q_j(x_0)-2a\delta_{j,0}\right\},$$

$$B^J=-\frac{Ga[J(J+1)]^{1/2}}{(2J+1)^2}[Q_{J-1}(x_0)-Q_{J+1}(x_0)].$$

C. Vector ($J^P=1^-$) Exchange

$$B_J=-G\left\{\left[3+\frac{(1+a^2)}{2a}\right]Q_J(x_0)-2(f/g)[(x_0-1)Q_J(x_0)-\delta_{J,0}]-\frac{2(f/g)^2}{(1-a)^2}[(x_0-1)(1+a+a^2+ax_0)Q_J(x_0)\right.$$
$$\left.-(1+a^2+ax_0)\delta_{J,0}-\tfrac{1}{3}a\delta_{J,1}]\right\}.$$

$$B_{JJ}=-G\left\{2Q_{J+1}(x_0)+2Q_{J-1}(x_0)+\frac{(1+2a+a^2-4ax_0)}{2a}Q_J(x_0)+2(f/g)[Q_{J+1}(x_0)+Q_{J-1}(x_0)-(x_0+1)Q_J(x_0)]\right.$$
$$\left.+\frac{(f/g)^2}{(1-a)^2}\{2(3a+x_0+2ax_0+a^2x_0+ax_0^2)Q_J(x_0)-(1+4a+a^2+2ax_0)[Q_{J+1}(x_0)+Q_{J-1}(x_0)]+\tfrac{4}{3}a\delta_{J,1}\}\right\}.$$

$$B_{J,J-1}=\frac{-G}{(2J+1)}\left\{\frac{1}{2a}[2J(1-a^2)+(1+a)^2]Q_{J-1}(x_0)+2(3J+1+Jax_0)Q_J(x_0)-2\left(\frac{f}{g}\right)\left[\frac{(4J+1+4Ja-a)}{(1-a)}Q_{J-1}(x_0)\right.\right.$$
$$\left.-\left((4J+1)+\frac{8Jax_0}{(1-a)}\right)Q_J(x_0)+\left(5+\frac{8ax_0}{1-a}\right)\delta_{J,1}\right]+\frac{(f/g)^2}{(1-a)^2}\{[(1+a^2)x_0+2J(x_0-1)(1-a^2)+6a]Q_{J-1}(x_0)$$
$$\left.+[4Ja^2x_0(x_0-1)+2(6J-1)a(x_0-1)-1-6a-a^2]Q_J(x_0)-(3+\tfrac{1}{3}a^2)\delta_{J,1}\}\right\}.$$

$$B_{J,J+1}=-\frac{G}{(2J+1)}\left\{\frac{1}{2a}[2(J+1)(1-a^2)-(1+a)^2]Q_{J+1}(x_0)+2[3J+2+(J+1)ax_0]Q_J(x_0)-2a\delta_{J,0}\right.$$
$$-2(f/g)\left[\left(\frac{4(J+1)(1+a)}{(1-a)}-1\right)Q_{J+1}(x_0)-\left(4J+3+\frac{8(J+1)ax_0}{(1-a)}\right)Q_J(x_0)+\frac{8a}{(1-a)}\delta_{J,0}\right]$$
$$-\frac{(f/g)^2}{(1-a)^2}[(x_0(1+a^2)-2(J+1)(1-a^2)(x_0-1)+6a)Q_{J+1}(x_0)$$
$$\left.-(1+6a+a^2+2a(6J+7)(x_0-1)+4(J+1)a^2x_0(x_0-1))Q_J(x_0)+(14a+4a^2(x_0-1))\delta_{J,0}+(8a^2/3)\delta_{J,1}]\right\}.$$

$$B^J=\frac{G[J(J+1)]^{1/2}}{(2J+1)^2}\left\{2(2J+1)(x_0-1)Q_J(x_0)+(1+a)[Q_{J-1}(x_0)-Q_{J+1}(x_0)]\right.$$
$$+2\left(\frac{f}{g}\right)\left[2(2J+1)(x_0-1)Q_J(x_0)+\frac{(1+3a)}{(1+a)}[Q_{J-1}(x_0)-Q_{J+1}(x_0)]\right]+\frac{(f/g)^2}{(1-a)^2}$$
$$\left.\times\{2(2J+1)(1-a)^2(x_0-1)Q_J(x_0)+(1+6a-a^2+2a^2x_0)[Q_{J-1}(x_0)-Q_{J+1}(x_0)]-2a^2\delta_{J,1}\}\right\}.$$

The coupling constants (g's and $\frac{2}{3}$'s) are defined in Ref. 5.